Energy & Environmental Science

PAPER

View Article Online
View Journal | View Issue

Cite this: *Energy Environ. Sci.*, 2018, **11**, 1271

Pushing the limit of layered transition metal oxide cathodes for high-energy density rechargeable Li ion batteries†

U.-H. Kim, ‡[a] D.-W. Jun,‡[a] K.-J. Park,[a] Q. Zhang,[b] P. Kaghazchi, [bh] D. Aurbach,*[c] D. T. Major,[c] G. Goobes,[c] M. Dixit, [c] N. Leifer,[c] C. M. Wang,[d] P. Yan,[d] D. Ahn, [e] K.-H. Kim, [f] C. S. Yoon*[g] and Y.-K. Sun *[a]

Received 23rd January 2018,
Accepted 6th March 2018

DOI: 10.1039/c8ee00227d

rsc.li/ees

Development of advanced high energy density lithium ion batteries is important for promoting electro-mobility. Making electric vehicles attractive and competitive compared to conventional automobiles depends on the availability of reliable, safe, high power, and highly energetic batteries whose components are abundant and cost effective. Nickel rich $Li[Ni_xCo_yMn_{1-x-y}]O_2$ layered cathode materials ($x > 0.5$) are of interest because they can provide very high specific capacity without pushing charging potentials to levels that oxidize the electrolyte solutions. However, these cathode materials suffer from stability problems. We discovered that doping these materials with tungsten (1 mol%) remarkably increases their stability due to a partial layered to cubic (rock salt) phase transition. We demonstrate herein highly stable Li ion battery prototypes consisting of tungsten-stabilized Ni rich cathode materials ($x > 0.9$) with specific capacities >220 mA h g^{-1}. This development can increase the energy density of Li ion batteries more than 30% above the state of the art without compromising durability.

Broader context

Although the global market share of electric vehicles (EVs) is estimated to grow sharply in the coming years, the main impediment for such a growth is the inadequate energy density and lifetime of the Li-ion-batteries (LIBs) that are currently powering most EVs in the market. Out of the components that composes LIBs, the cathode primarily limits the battery's overall energy density and lifetime. In this paper, we demonstrate that $LiNiO_2$ cathodes which have been largely ignored because of their rapid capacity fading, can be used as high-capacity cathodes that can satisfy the energy demands for EVs. Our newly prepared $LiNiO_2$ cathodes can deliver an unprecedented high specific capacity (247 mA h g^{-1}) at 4.3 V. More importantly, doping $LiNiO_2$ with W at a low level (1 mol%) drastically increases its cycling stability (90% of the initial discharge capacity after 100 cycles) as well as the thermal stability. Furthermore, the beneficial effects of the W-doping are extended to all kinds of Ni-rich $Li[Ni_xCo_yMn_{1-x-y}]O_2$ cathodes with $x \geq 0.8$ by improving their respective cycling stability, demonstrated during 1000 cycles in full-cells testing. Hence, we show the results reported herein reflect a leap forward compared to previously published data on Ni-rich cathodes.

[a] *Department of Energy Engineering, Hanyang University, Seoul, 04763, South Korea. E-mail: yksun@hanyang.ac.kr*
[b] *Physiklische und Theoretische Chemie, Freie Universitat, Berlin, D-14195, Germany*
[c] *Department of Chemistry and BINA (BIU institute of nano-technology and advanced materials), Bar-Ilan University, Ramat-Gan, 5290002, Israel. E-mail: aurbach@mail.biu.ac.il*
[d] *Energy and Environmental Directorate, Pacific Northwest National Laboratory, 902 Battelle Boulevard, Richland, WA 99352, USA*
[e] *PLS-II Beamline Division, Pohang Accelerator Laboratory (PAL), Pohang, 37673, South Korea*
[f] *Global Frontier Center for Hybrid Interface Materials, Pusan National University, Busan 609-735, South Korea*
[g] *Department of Materials Science and Engineering, Hanyang University, Seoul, 04763, South Korea. E-mail: csyoon@hanyang.ac.kr*
[h] *Forschungszentrum Jülich GmbH, Institute of Energy and Climate Research (IEK-1), Materials Synthesis and Processing, Wilhelm-Johnen-Straße, 52425 Jülich, Germany*

† Electronic supplementary information (ESI) available. See DOI: 10.1039/c8ee00227d

‡ These authors contributed equally to this work.

1. Introduction

First introduced in 1992, $LiCoO_2$ (LCO) was the first layered transition metal oxide to be successfully incorporated into commercial rechargeable Li-ion batteries (LIBs). LCO and other layered transition metal oxide cathodes[1–5] are still used widely in portable electronic devices as positive electrodes. Despite the success of LIBs, there has been a strong impetus to lower the material cost and increase the specific capacity of the cathodes, especially for electric vehicles (EVs), which require high specific energy density to meet the drive range requirement per single charge. The current strategy for increasing capacity in LCO type layered cathodes is to increase the Ni-content in $Li[Ni_xCo_yM_{1-x-y}]O_2$ (M = Al or Mn) cathodes (*e.g.*, LCO (150 mA h g^{-1}) → $Li[Ni_{1/3}Co_{1/3}Mn_{1/3}]O_2$ (160 mA h g^{-1}) → $Li[Ni_{0.6}Co_{0.2}Mn_{0.2}]O_2$ (185 mA h g^{-1}) → $Li[Ni_{0.8}Co_{0.1}Mn_{0.1}]O_2$ (200 mA h g^{-1})).[6]

At the extreme end of this Ni-enrichment strategy, $LiNiO_2$ (LNO) is an attractive cathode material because it has a theoretical capacity of 275 mA h g^{-1} and relatively low materials cost. In the 1990s, there was extensive testing of LNO as a cathode for LIBs.[7–11] In fact, Arai *et al.* extracted 260 mA h g^{-1} at 4.5 V *vs.* Li (95% of the theoretical capacity); however, the high discharge capacity could not be maintained upon cycling and lost 24% of the initial capacity after the first cycle.[10] It is also notoriously difficult to prepare stoichiometric LNO because high-temperature treatment often leads to Li-deficiency or conversion of LNO to $Li_{1-x}Ni_{1+x}O_2$ with partial disordering of cations that are presumed to be electrochemically inactive.[9,12,13] High level of cation disordering characterized LNO cathode materials presented in earlier works, resulted from syntheses by solid state reactions. However, in the present work mono-disperse spherical $Ni(OH)_2$ precursor particles were first synthesized through solution-precipitation in a specially designed reactor. The hydroxide precursors were lithiated under high-purity oxygen atmosphere by calcination at 650 °C (optimized by trial and error) with 1% excess $LiOH{\cdot}H_2O$. Through this two-step synthesis, the cation mixing (disordering) was reproducibly kept around ~2%,[14–17] what ensured the production of high quality cathode material.

LNO was also found to be highly surface reactive in all kinds of electrolyte solutions relevant to LIB.[18] The reversible discharge capacity of LNO had to be limited to 150 mA h g^{-1} by cycling below 4.2 V due to its structural instability at high charge voltages.[9] Here, we show that an unprecedented high specific capacity can be delivered by newly prepared LNO charged up to 4.3 V, which is well below the anodic breakdown limit of the electrolyte solutions. Doping LNO with W at low level (1 mol%) also drastically increases its stability, which allowed us to take advantage of the very high specific capacity of LNO cathodes. Furthermore, we demonstrate that the beneficial effect of the W-doping extends to all Ni-rich $Li[Ni_xCo_yMn_{1-x-y}]O_2$ cathodes with $x \geq 0.8$. We show that the results reported herein reflect a leap forward compared to previously published data on Ni rich cathode materials.

2. Experimental

2.1 Synthesis of W-doped $Li[Ni_xCo_yMn_{1-x-y}]O_2$

Spherical W-doped $[Ni_xCo_yMn_{1-x-y}](OH)_2$ precursors (x = 0.8, 0.89, 0.9 and 1.0; y = 0.15, 0.11, 0.05 and 0) were synthesized *via* a co-precipitation method. Appropriate amounts of $NiSO_4{\cdot}6H_2O$, $CoSO_4{\cdot}7H_2O$, and $MnSO_4{\cdot}H_2O$ were pumped into a batch reactor (47 L) filled with a solution of NH_4OH (aq) and NaOH (aq) under a replenished nitrogen atmosphere. Concurrently, 4 M WO_3-dissolved NaOH (aq) (molar ratio of sodium hydroxide to transition metal = 2.0) and a NH_4OH chelating agent (aq) (molar ratio of ammonium hydroxide to transition metal = 1.2) were fed separately into the reactor. During the early stage of the co-precipitation reaction, nano-sized spherical $[Ni_xCo_yMn_{1-x-y}](OH)_2$ particles were formed first and then nickel–cobalt–manganese-tungsten hydroxides slowly accumulated on the surfaces of the formed hydroxide particles, leading to micro-sized particle after 27 h. Powder of these particles was obtained through filtering, washing, and drying at 110 °C overnight. The obtained W-doped $[Ni_xCo_yMn_{1-x-y}](OH)_2$ hydroxide powder as a precursor was thoroughly mixed with $LiOH{\cdot}H_2O$ (Li:(Ni + Co + Mn + W) = 1.01 : 1 molar ratio) and then calcined at various temperatures depending on the composition for 10 h in flowing oxygen.

2.2 Material characterization

The chemical composition of the LNO powder was verified using inductively coupled plasma spectrometry (ICP-OES, OPTIMA 8300). Scanning electron microscopy (JSM-6340F) and transmission electron microscopy (JEOL 2100F and aberration-corrected FEI 300 kV Titan) were used to examine the morphology and microstructure of the cathodes. TEM samples were prepared by focused ion beam. Powder X-ray diffraction analysis was carried out at 9B High Resolution Powder Diffraction Beamline at Pohang Accelerator Laboratory. Methods for the theoretical calculation of the W-doped LNO structure are explained in the ESI.†

2.3 Electrochemical measurements

For electrochemical testing, pristine and W-doped $Li[Ni_xCo_yMn_{1-x-y}]O_2$ (x = 0.8, 0.89, 0.9 and 1.0; y = 0.15, 0.11, 0.05, and 0) powders were mixed with carbon black and poly(vinylidene fluoride) in a weight ratio of 90 : 5.5 : 4.5 in *N*-methyl-2-pyrrolidone. The slurry was spread onto an Al foil with an active material loading level of 4–5 mg cm^{-2} (for both half and full cells), dried and roll-pressed. Cell tests were performed at 0.5C-rate (90 mA g^{-1}) at 30 °C in a 2032 coin-type half-cell using lithium metal anode and 1.2 M $LiPF_6$ in ethylene carbonate–ethyl methyl carbonate (EC : EMC = 3 : 7 by vol%) with 2 wt% vinylene carbonate (VC) as electrolyte. For full cell testing, a laminated-pouch-type full-cell (30 mA h) was used. The commercial graphite (MCMB, Osaka Gas) was used as the anode. Full-cells capacity balance (N/P ratio) was in the range of 1.15–1.20. The cells were charged and discharged between 3.0 and 4.2 V by applying a constant 1C current (200 mA g^{-1}) at 25 °C. Electrochemical impedance spectroscopy measurements were performed using 2032 coin-type half-cells by a multi-channel potentiostat (Bio-Logic, VMP3) over the frequency range from 1.0 mHz to 1.0 MHz with a voltage amplitude of 10 mV.

2.4 Thermal stability measurements

For thermal stability measurement, 2032 coin-type half-cells were charged at constant voltage of 4.3 V *versus* Li metal anode and disassembled to recover the cathodes in an Ar-filled dry box. The electrodes were washed with dimethyl carbonate and dried and then active materials were scraped from the cycled electrodes. Stainless steel sealed pan with gold-plated copper seals were used to accommodate 7 mg samples with 200 μL fresh electrolyte solution (1.2 M $LiPF_6$ in EC : EMC = 3 : 7 by vol% + 2 wt% VC). The measurements were performed using a DSC 214 polyma (Netzsch, Germany) at a temperature scan rate of 5 °C min^{-1}.

3. Results and discussion

The selection of an appropriate synthetic route is critically important. LNO was synthesized by precipitating spherical $Ni(OH)_2$ precursor particles using a specially designed 47 L batch-type reactor followed by lithiation through high-temperature calcination of the mixture of excess $LiOH{\cdot}H_2O$ and the hydroxide precursor as described in ref. 19 and 20. Pre-shaping of the $Ni(OH)_2$ precursors into spherical particles composed of nano-sized primary particles helps to minimize the contact of the reactive Ni-rich surface with the electrolyte solution, while abundant grain boundaries within each particle facilitate the Li^+ diffusion of ions into the particle interiors (see morphological data Fig. S1, ESI†). For W-doped LNO samples, W was introduced in the Ni hydroxide precursor stage to ensure uniform distribution of W throughout the primary particles. Structural analysis by X-ray diffraction (XRD), high-resolution transmission electron microscopy (HRTEM) and selected area electron diffraction (SAED), revealed that the LNO material is composed of a major hexagonal layered phase ($R\bar{3}m$) and a minor (a few percent) rock-salt phase ($Fm\bar{3}m$), produced from manifestation of partial cation mixing on the transition metal sites in the $R\bar{3}m$ lattice. The concentration of the latter is higher, close to the particles surface, as evidenced by HRTEM analysis (Fig. 1 and Fig. S2, ESI†). Such two-phase mixture was also previously observed with XRD when LNO was heat treated at high temperatures.[9,16,21] Structural analyses clearly show that the percentage of the rock-salt phase increases with the amount of W in the active mass. XRD diffraction data and analysis for LNO and W-doped LNO samples are provided in Fig. S3 and Table S1 (ESI†). The refinement produced the best fitting result as a two-phase mixture (layered $LiNiO_2$ and partially cation-disordered $Fm\bar{3}m$ $Li_{1-x}Ni_{1+x}O_2$) with the fraction of the $Fm\bar{3}m$ phase tending to increase with higher W-doping level, which was also confirmed by the increased Li–O bond distance coupled with a concurrent decrease in the Ni–O distance as the W doping level was increased. Such a change in Li–O and Ni–O bond distances was correlated to either increasing cation disorder or the presence of a rocksalt phase.[16] Fig. 1a shows an HRTEM image of a W-doped LNO sample close to the surface, exhibiting clear segregation between a surface rocksalt $Fm\bar{3}m$ phase and a bulk $R\bar{3}m$ phase. The insets show Fourier filtered images of each phase at atomic resolution. The presence of the rocksalt $Fm\bar{3}m$ was typically observed in cycled or damaged Ni-enriched $Li[Ni_xCo_yMn_{1-x-y}]O_2$ cathodes, but was not often observed in the as-prepared state. Furthermore, the rocksalt phase was not confined to the surface as thin layer; instead, SAED analysis indicates that the entire primary particles possess the $Fm\bar{3}m$ symmetry. To clarify the existence of the rocksalt phase in the W-doped LNO cathode materials, electron diffraction patterns from each phase obtained in two diffraction zones (together with the corresponding bright field images) are shown in Fig. S2 (ESI†). The [100] rocksalt zone pattern changed to the [110] rocksalt zone after tilting the sample by 45°, which is in agreement with the cubic symmetry. In contrast, the [010] layered pattern became a [120] layered zone by tilting the sample by 30°, which is consistent with the symmetry of the layered structure as illustrated in Fig. S2 (ESI†). To estimate the distribution of the rocksalt phase, phase mapping of representative particles of the LNO and W-doped materials (0.5 mol% and 1 mol%) was carried out using ASTAR (automatic TEM phase-identification/orientation mapping technique). Fig. 1b shows a typical result, illustrating the distribution of the rock-salt phase within the particles. To add credibility to the ASTAR analysis, the phase distribution was also manually confirmed using SAED on the same specimen, and an example of this for 1 mol% W-LNO is shown in the charts of Fig. 1c. The rocksalt phase was initially uniformly distributed in the LNO particles and increasingly segregated at the surface of the particles at higher W doping levels. In addition, increasing the level of W doping increased the relative fraction of the rock-salt phase, which agrees with the XRD data. As further proof of the two-phase mixture,[6] Li magic-angle spinning nuclear magnetic resonance (NMR) spectroscopy of the pure and doped LNO was carried out. Both spectra in Fig. S4 (ESI†) exhibit a main peak at ~660 along with a small peak at 425 ppm. The resonance value of this latter peak is consistent with the rocksalt phase, upon consideration of the average oxidation state of the nickel ions.[7] This peak increase from approximately 4 to 8% in the pure and 1% doped material, respectively. Hence, the NMR results support the structural analysis, which indicates that W doping indeed increases the amount of the rock salt phase in the LNO active mass.

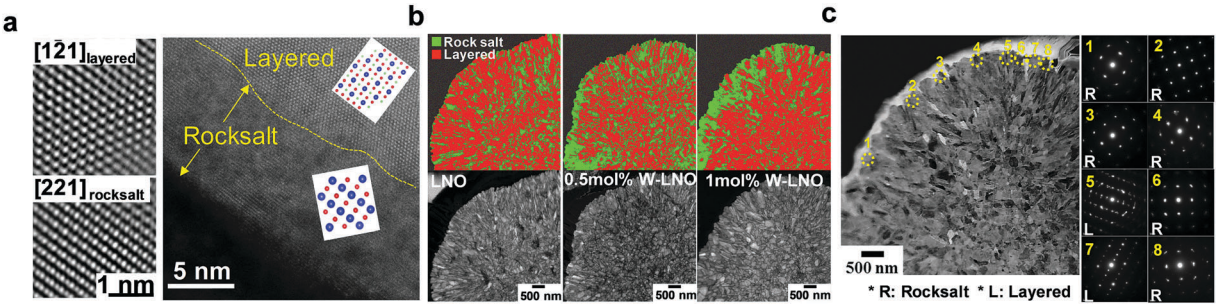

Fig. 1 (a) HRTEM image of 1 mol% W-LNO of surface rocksalt $Fm\bar{3}m$ and bulk $R\bar{3}m$ phases. The insets show Fourier filtered images of each phase at an atomic resolution. (b) ASTAR TEM phase mapping and corresponding bright field images for LNO, 0.5 mol% and 1 mol% W-LNO, showing distribution of the rocksalt phase in the respective cathode. (c) Electron diffraction patterns from 8 primary particles on the periphery of the 1 mol% W-LNO particle confirms the ASTAR phase mapping data shown in (b), showing the surface segregation of the rocksalt phase for the W-doped LNO cathode.

To understand the theoretical basis for the increased rock salt formation due to W-doping, density functional theory was used to compute the total energies of the ideal bulk $Fm\bar{3}m$ (cation-disordered) and $R\bar{3}m$ (fully-ordered) LNO structures. To make a direct comparison between energies of these phases we have modelled the bulk structure with the same number of atoms (96 Li, 96 Ni, 192 O). The energy difference (per formula unit) between the two structures (−21.88 eV for $Fm\bar{3}m$ and −21.89 eV for $R\bar{3}m$) was very small. The calculation was repeated with 2 mol% replacing Li sites for the $Fm\bar{3}m$ and $R\bar{3}m$ structures. 2 mol% W was used to amplify the doping effect. The calculation result summarized in Fig. S5 (ESI†) indicates that the energies for both structures were almost identical within the accuracy of the calculation, suggesting that either $Fm\bar{3}m$ or $R\bar{3}m$ phases can be stabilized in LNO.

To theoretically substantiate the surface segregation of the rocksalt phase, surface energies of the two structures were calculated. To study surfaces of the rocksalt and the hexagonal layered phase of LNO, we focused on (001) and (10$\bar{1}$4) orientations as most abundant facets of rocksalt crystals are generally {001}[22,23] and the (10$\bar{1}$4) surface has been found to be the most energetically favorable stoichiometric nonpolar surface for the layered phase.[24,25] Since surface energies of these surfaces are low, they are expected to have high contributions to the primary particles of LNO. To calculate and compare surface energies with high accuracy, we have considered the same number of Li, Ni, O, and W atoms for both phases as well as the same unit cell for bulk and surface in each case. To study the influence of the level of delithiation on the stability and O removal energy we modelled bulk and surfaces of Li_xNiO_2 with Li content of x = 1.00, 0.50, and 0.25. The W-doped bulk and surfaces of LNO have been modelled considering 2% dopant (2 W per 96 Li sites). The W dopants have been accommodated to subsurface layers in order to avoid a direct effect of W on the O release energy. To calculate surface energies for pristine and W-doped Li_xNiO_2 cases with x = 1.00, 0.50, and 0.25, unit cells and atomic coordinates in respective bulk phases were first fully optimized. To model the surfaces, the unit cell dimensions in a and b directions (surface plane directions) were kept fixed and a vacuum space of 12 Å was introduced to the c direction (perpendicular to the surface plane) and then atomic coordinates were optimized. Computed surface energies for the rock salt Li_xNiO_2(001) are lower than those of the layered Li_xNiO_2(10$\bar{1}$4) with and without W-doping for all considered Li contents as shown in Fig. 2. The surface energy of the LNO surfaces increases with the reduction of Li content, which is due to the reduced atomic coordination at the surface. W doping increases surface energies of the layered LNO(10$\bar{1}$4), but it decreases those of rocksalt LNO(001). This result shows that formation of W-doped rocksalt surfaces are energetically favored compared to the bare rocksalt surfaces as well as the layered surfaces. The theoretical calculation suggests that W-doping promotes segregation of the rocksalt phase on the surface. Effect of W-doping on the oxygen removal energy from the LNO surfaces was also studied. Calculation of the oxygen release energy was exclusively based on $Li_{0.25}NiO_2$. As can be seen in Fig. 2, there are two

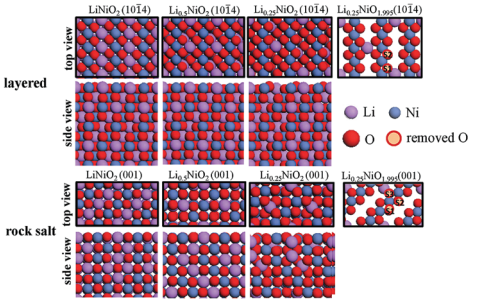

	Surface energy(meV / Å²)						O Release energy (eV)	
	$LNiO_2$		$Li_{0.5}NiO_2$		$Li_{0.25}NiO_2$		$Li_{0.25}NiO_{1.995}$	
	Pristine	2% W →Li	Pristine	2% W →Li	Pristine	2% W →Li	Pristine	2% W →Li
(10$\bar{1}$4)	40.0	40.5	66.9	68.7	72.9	73.6	1.11	0.96
(001)	31.7	31.3	57.1	55.7	56.6	56.3	1.24	1.33

Fig. 2 Top and side views of atomic structures of hexagonal layered (10$\bar{1}$4) and rocksalt (001) surfaces of Li_xNiO_2 with x = 1.00, 0.50, and 0.25. The right panel figures are top views of the topmost layer of $Li_{0.25}NiO_{1.995}$ showing different distinguishable surface O vacancy sites. Calculated surface energies for layered Li_xNiO_2(10$\bar{1}$4) and rock salt Li_xNiO_2(001) as well as O release energies from the most favorable vacant sites (S2 in both cases) on $Li_{0.25}NiO_2$(10$\bar{1}$4) and $Li_{0.25}NiO_2$(001) before and after 2% W doping are listed in the bottom table.

distinguishable surface oxygen sites on the layered surface and three distinguishable surface O sites on the rocksalt surface. Focusing on the most favorable O vacancy site at each surface (Fig. S2, ESI,† in both cases), we calculated the oxygen release energy and found that oxygen removal from the surface of rocksalt is less favorable than that of the layered phase with and without W doping. W dopant decreases oxygen release energy from the layered surface, but it increases oxygen release energy from the rocksalt surface. In addition, investigation of the local magnetic moments and spin directions of Ni in ideal and cation disordered structures indicate that Ni^{3+} ions are partially reduced to Ni^{2+} due to charge compensation after doping W^{6+} at Ni^{3+} sites. This will reduce the amount of Jahn–Teller active ions in the material, and likely stabilizes the structure (Table S2, ESI†). In conclusion, the computer modelling shows that W-doping energetically favors the rocksalt phase formation near the surface, and its presence also adds chemical stability to the cathode surface by suppressing oxygen release, thus mitigating the capacity fading observed with the undoped LNO cathodes.

Fig. 3a and b provide typical cycling data of the cathode materials studied herein *vs.* Li metal anodes, while Fig. 3c provides cycling data of these cathodes *vs.* graphite anodes (Pouch-type full cells, Li ion battery prototypes). The first charge capacity of LNO cathodes is around 255 mA h g^{-1} at a 0.1C rate with a high first-cycle coulombic efficiency of 97% as seen from the first charge–discharge curves in Fig. 3a. The previously reported first-cycle efficiency of LNO cathodes was limited to ~85%[10,18] due to high irreversible capacity loss. The capacity extracted from the LNO cathode prepared for this study represents one of the highest values ever observed for a layered transition metal oxide cathode at a maximum charging

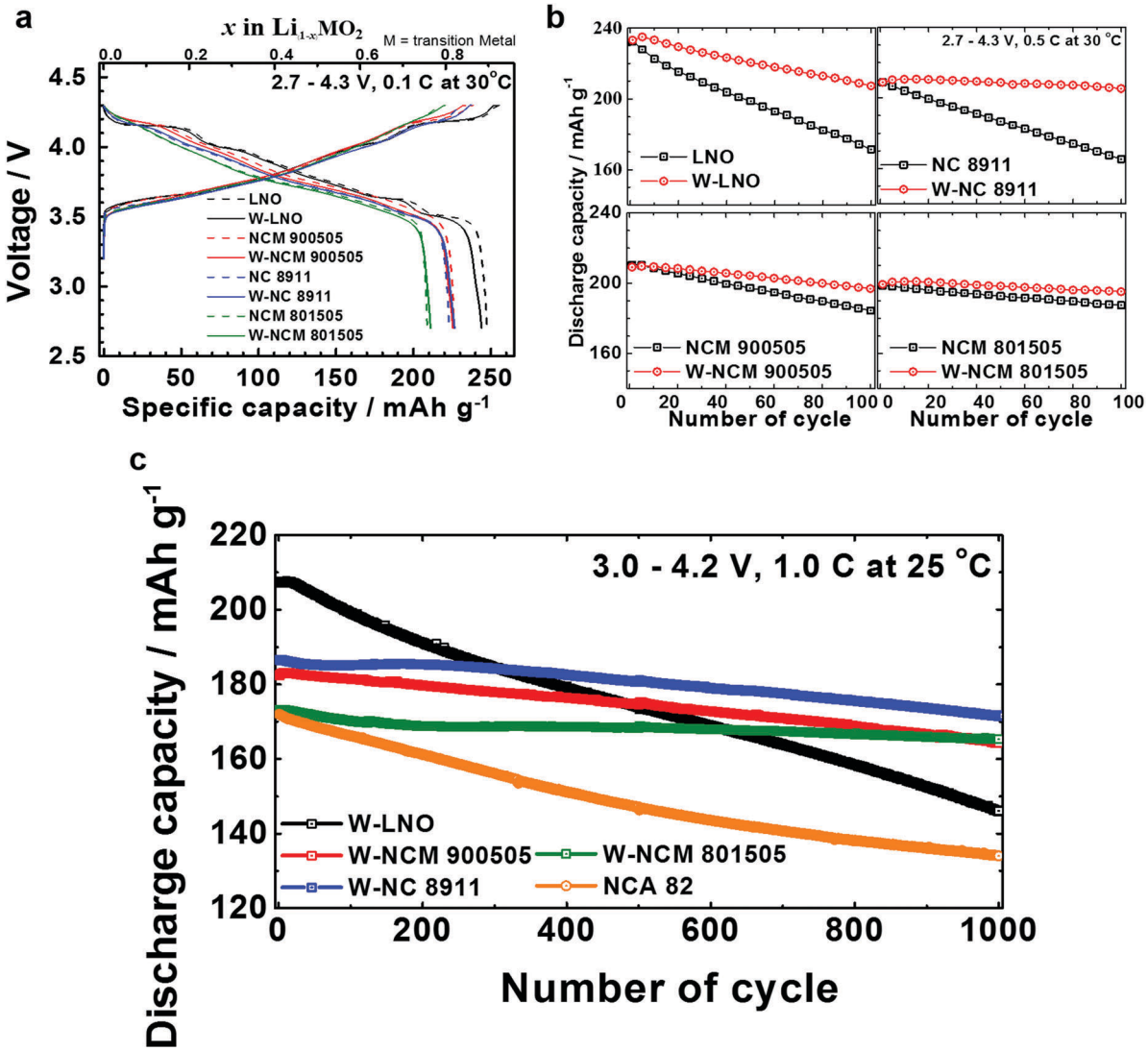

Fig. 3 Electrochemical performance of the W-doped $Li[Ni_xCo_yMn_{1-x-y}]O_2$ including LNO: (a) 1st cycle voltage profiles for pristine and 1 mol% W-doped $Li[Ni_xCo_yMn_{1-x-y}]O_2$ with x = 0.8, 0.89, 0.9 and 1.0; y = 0.15, 0.11, 0.05, and 0 cathodes (W-NCM 801505, W-NC 8911, W-NCM 900505, and W-LNO). All cells are operated within a voltage range of 2.7–4.3 V at 0.1C and 30 °C in a half cell using Li metal anode. (b) Cycling performance of the cathodes in (a), tested at 0.5C. (c) Long term cycling of 1 mol% W-doped $Li[Ni_xCo_yMn_{1-x-y}]O_2$ with x = 0.8, 0.89, 0.9 and 1.0; y = 0.15, 0.11, 0.05, and 0 cathodes and $Li[Ni_{0.82}Co_{0.14}Al_{0.04}]O_2$ (NCA 82, commercial Ni rich benchmark cathode) for comparison, tested using pouch cells at 1.0C and 25 °C within a voltage range of 3.0–4.2 V against graphite anodes.

potential of 4.3 V. This translates to a specific energy density (cathode only) of 865 W h kg^{-1} compared to 540 W h kg^{-1} for LCO and 704 W h kg^{-1} for $Li[Ni_{0.8}Co_{0.15}Al_{0.05}]O_2$ (denoted as NCA). The Coulombic efficiency stabilizes around 100% after the first cycle; however, a capacity fading, typical of LNO, is observed during cycling (on average around 0.25% per cycle, 74% of the initial discharge capacity after 100 cycles) as shown in Fig. 3b. Doping of LNO with W slightly decreases the initial discharge capacity to 245 mA h g^{-1} with a first-cycle Coulombic efficiency of 96%, but the main improvement of the LNO cathode by W doping is the remarkable stabilization, reflected by impressive capacity retention as seen in Fig. 3b. The 1 mol% W-LNO cathode exhibits capacity retention approaching 90% after 100 cycles. Remarkably, the specific discharge capacity for the 1 mol% W-LNO cathode even after 100 cycles averages around 210 mA h g^{-1}, which is still larger than the maximum reported values for Ni rich benchmark commercial NCA cathodes. The electrochemical analysis of these cathodes ($dQ\ dV^{-1}$ *vs.* V curves related to galvanostatic processes, Fig. S6, ESI†) reflects the phase transition processes that the LNO cathodes undergo during charging/discharging, indicating that capacity is obtained from the Ni^{3+}/Ni^{4+} redox couple. However, the $dQ\ dV^{-1}$ curve for the LNO cathode progressively deteriorated during cycling, while the W-doped LNO cathodes maintained the initial $dQ\ dV^{-1}$ curve, preserving the structural integrity upon repeated phase transitions that accompany Li insertion and removal. As shown in Fig. S6 and S7 (ESI†), the improvement in the cycling stability of the LNO cathode due to doping with W depends on the W concentration. The level of stability follows the order of 1 mol% > 0.5 mol% > 0% W doping based on the overlapping $dQ\ dV^{-1}$ *vs.* V curves

(Fig. S6, ESI†) and the decrease in the capacity fading per cycle (Fig. S7, ESI†). The improvement in the cycling stability, however, plateaued at 1 mol% as the 1.5 mol% W-LNO cathode (data not shown here) showed no further improvement, indicating that the 1 mol% W doping is optimal. The effect of W doping on other Ni rich cathode materials ($Li[Ni_xCo_yMn_{1-x-y}]O_2$ with x = 0.8, 0.89 and 0.9; y = 0.15, 0.11 and 0.05) is also included in Fig. 3a and b. Like the LNO cathode, 1 mol% W doping hardly affected the initial specific capacities of the Ni-rich $Li[Ni_xCo_yMn_{1-x-y}]O_2$ cathodes. Regardless of the Ni concentration, W doping leads to an impressive improvement in stability upon cycling. This effect of doping is stronger as the level of Ni increases. Especially, in the case of the 1 mol% W-doped $Li[Ni_{0.89}Co_{0.11}]O_2$ even without the cycle-stabilizing Mn ions in the composition, the cathode hardly exhibited any capacity loss at the end of 100 cycles when doped with W ions. The propitious effect of the W doping on cycling stability extended to long-term cycling of the $Li[Ni_xCo_yMn_{1-x-y}]O_2$ cathodes. Pouch cells, which are Li-ion battery prototypes (against graphite anodes) containing W-doped $Li[Ni_xCo_yMn_{1-x-y}]O_2$ (x = 0.8, 0.89, 0.9 and 1.0; y = 0.15, 0.11, 0.05, and 0) cathodes also demonstrated impressive stability over many hundreds of cycles (Fig. 3c). An important comparison between the Li ion cells containing 1 mol% W-doped $Li[Ni_{0.8}Co_{0.15}Mn_{0.05}]O_2$ and $Li[Ni_{0.82}Co_{0.14}Al_{0.04}]O_2$ (NCA, a commercial Ni rich benchmark cathode with similar Ni content and similar initial specific capacity, deployed in a commercial EV) is presented in Fig. 3c. After 1000 cycles, the NCA cell loses nearly 25% of its capacity and hence, in a commercial EV, the depth of discharge (DOD) is typically limited to 60 to 70% to counter the capacity fading problem.[26] In comparison, the W-doped $Li[Ni_{0.8}Co_{0.15}Mn_{0.05}]O_2$ cathode shows nearly no drop in specific capacity even after 1000 cycles at full DOD, and the cell is projected to continue to cycle stably well beyond 1000 cycles. A comparison of these results to those obtained by extensive parallel studies of Ni rich cathode materials doped with other elements (*e.g.* Zr, Ti, and Mo) shows that doping with W provides the highest level of stabilization (Fig. S8, ESI†). It is important to examine how doping by W affects stability as reflected by the evolution of the electrodes impedance during cycling. Impedance spectra of LNO and W-LNO cathodes measured after the 1st, 25th, 50th, 75th and 100th cycles (Fig. 4) indicate that 1 mol% W-LNO cathodes exhibits a much smaller overall impedance and stable behavior compared to undoped LNO cathodes, for which the impedance markedly increased upon cycling. The high frequency surface film resistance for both the LNO and 1 mol% W-LNO cathodes was similar in magnitude; however, more pronounced differences are observed in the medium-low frequency features of these electrodes' spectra. It increases by 13-fold (6 to 79.5 Ω) for the LNO cathodes during 100 cycles, while for the W-LNO the increase in the medium frequency semicircle upon cycling is by far smaller (spectacular in Fig. 4). These impedance results clearly affirm that the W-LNO particles are more robust and stable upon cycling and that the charge transport properties of the W-LNO cathodes are better than that of LNO cathodes. Another clear and important message from these impedance measurements is that W-doping of LNO has both surface and bulk effects. W-doping also lowers the impedance of 1 mol% W-$Li[Ni_xCo_yMn_{1-x-y}]O_2$ with x = 0.8 and 0.9, thus confirming that W-doping brings a general enhancement in charge transport properties for a range of layered $Li[Ni_xCo_yMn_{1-x-y}]O_2$ cathodes with the effect becoming more notable with higher Ni fractions.

Another important aspect discussed herein is thermal stability consideration (*i.e.* safety features), which is often mentioned as a great concern for Ni rich $Li[Ni_xCo_yMn_{1-x-y}]O_2$ cathodes. The thermal behavior of the above mentioned W-doped and un-doped $Li[Ni_xCo_yMn_{1-x-y}]O_2$ cathode materials in contact

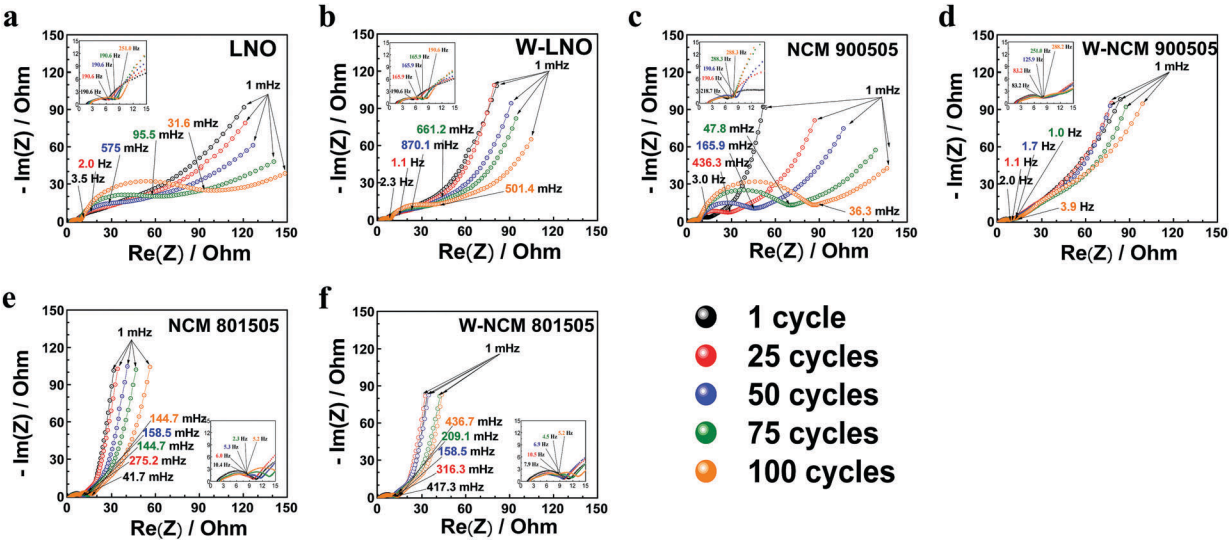

Fig. 4 Nyquist plots of electrochemical impedances of the W-doped $Li[Ni_xCo_xMn_{1-x-y}]O_2$ cathodes measured at the fully charged state, around 4.3 V, after the 1st, 25th, 50th, 75th and 100th cycles: (a) LNO, (b) 1 mol% W-LNO, (c) NCM 900505, (d) 1 mol% W-NCM 900505, (e) NCM 801505, and (f) 1 mol% W-NCM 801505.

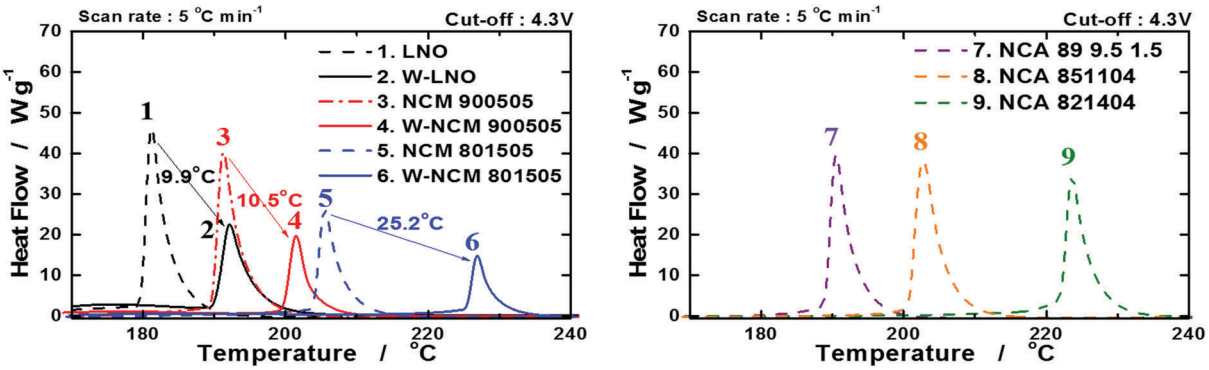

Fig. 5 DSC results of the pristine, W-doped $Li[Ni_xCo_yMn_{1-x-y}]O_2$ (x = 0.8, 0.9 and 1.0; y = 0.15, 0.05, and 0) and benchmarking cathode materials: (NCA 89 9.5 1.5, NCA 851104 and NCA 821404) together with 1.2 M $LiPF_6$, EC/EMC 3 : 7 by vol% + 2 wt% VC electrolyte solutions, demonstrating that W-doping significantly improves the thermal stability of the $Li[Ni_xCo_yMn_{1-x-y}]O_2$ cathodes. Peak temperature and the enthalpy released from the exothermic reactions with the electrolyte solutions are listed in Table 1.

with the electrolyte solutions used herein was measured by differential scanning calorimetry. For comparison the thermal behavior of benchmark – reference cathode materials $Li[Ni_{0.89}Co_{0.095}Al_{0.015}]O_2$, $Li[Ni_{0.85}Co_{0.11}Al_{0.04}]O_2$ and $Li[Ni_{0.82}Co_{0.14}Al_{0.04}]O_2$ (NCA) was measured as well in similar experiments, the results are presented in Fig. 5. It was clearly demonstrated that W-doping of these Ni rich layered cathode materials can substantially reduce their thermal activity by shifting the onset of their exothermic reactions with the electrolyte solutions upon heating by more than 10 °C and by decreasing the overall heat released from these thermal reactions (Fig. 5 and Table 1).

Hence, the presence of W ions in the layered $Li[Ni_xCo_yMn_{1-x-y}]O_2$ lattice indeed improves considerably their thermal stability regardless the Ni fraction in the compounds, what correlates well with the revolutionary positive effect of W doping on their electrochemical behavior, stability and their impedance features. Post mortem analyses of the LNO and 1 mol% W-LNO electrodes even after 100 cycles also show striking differences. Analysis of particles taken from cycled electrodes was carried out by scanning electron microscopy (SEM) and energy-dispersive X-ray spectroscopy (EDS) using a thin section prepared using a focused ion beam. The pristine LNO particles taken from cycled electrodes exhibit the usual detrimental morphological and chemical effects of cycling and eventual pulverization of the particles, typical of Ni rich $Li[Ni_xCo_yMn_{1-x-y}]O_2$ cathodes as shown in Fig. 6a.

In contrast, the 1 mol% W-LNO particles retained their spherical morphology with no noticeable structural degradation (Fig. 6b). EDS compositional mapping of the cross section of the cycle LNO particle in Fig. 6c shows a uniform distribution of F throughout the scanned area as the LNO particles are unavoidably exposed to acidic solution species such as HF and PF_5 present in the $LiPF_6$-base electrolyte. In the case of the cycled 1 mol% W-LNO cathode, hardly any F was detected within the particles, and the presence of F was confined to the particle periphery due to the surface precipitation of LiF, as can be seen from Fig. 6c. In addition, detailed TEM analysis shows that the cycled LNO cathode (Fig. 7) suffered severe structural damage, which progressively intensified near the surface and the NiO-like

Table 1 Results of peak temperature and enthalpy values using differential scanning calorimetry for W-doped $Li[Ni_xCo_yMn_{1-x-y}]O_2$ (x = 0.8, 0.9 and 1.0; y = 0.15, 0.05, and 0) and benchmarking cathode materials: (NCA 89 9.5 1.5, NCA 851104 and NCA 821404)

#	Sample	Peak temperature	Enthalpy
1	LNO	181.2 °C	1854 J g^{-1}
2	W-LNO	191.1 °C	1231 J g^{-1}
3	NCM 900505	190.9 °C	1261 J g^{-1}
4	W-NCM 900505	201.4 °C	1056 J g^{-1}
5	NCM 801505	204.8 °C	1204 J g^{-1}
6	W-NCM 801505	230.0 °C	949.5 J g^{-1}
7	NCA 89 9.5 1.5	189.7 °C	1931 J g^{-1}
8	NCA 851104	201.1 °C	1881 J g^{-1}
9	NCA 921404	222.8 °C	1727 J g^{-1}

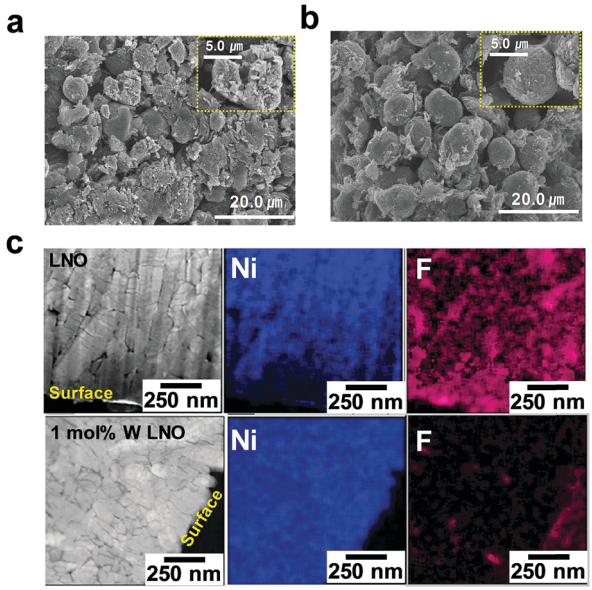

Fig. 6 (a) SEM image of cycled LNO electrode. (b) SEM image of cycled 1 mol% W-LNO cathode. (c) EDS elemental mapping of a particle from cycled LNO and 1 mol% W-LNO cathodes. All cells were cycled at 2.7–4.3 V and 0.5 C in a half cell *vs.* Li.

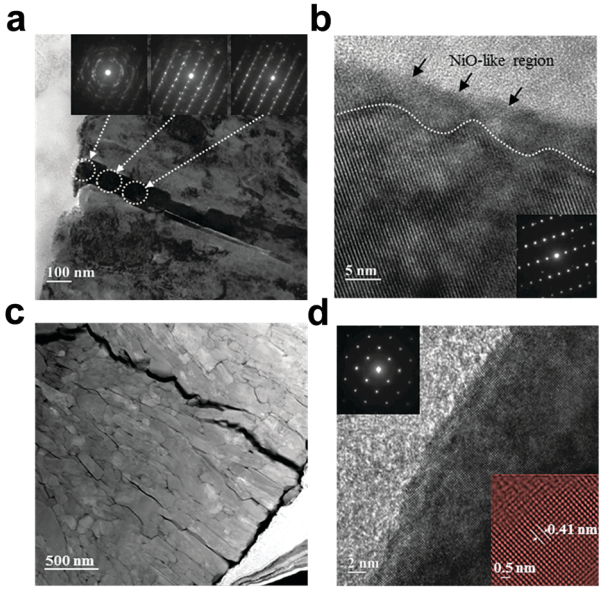

Fig. 7 (a) Bright field TEM image of the cycled LNO electrode with electron diffraction patterns along a damaged grain (inset highlight the secondary phases on the damaged surface). (b) $[010]_{layered}$ zone HR-TEM image of the cycled LNO showing the NiO-like phase. (c) HADDF image of the cycled LNO showing inter- and intra-cracks. (d) $[001]_{rocksalt}$ zone HRTEM image of the cycled 1 mol% W-LNO electrode with the inset showing the preserved cubic lattice at the surface.

surface region. This phenomenon is often cited as a cause for the increase in the charge transfer resistance and subsequent capacity degradation for Ni-rich NCA or $Li[Ni_xCo_yMn_{1-x-y}]O_2$ cathodes.[26–28] In addition to the surface damage incurred during cycling, numerous inter- and intra-granular cracks were observed in TEM images of cycled LNO electrode (Fig. 7), likely resulting from the large shrinkage in the interlayer distance towards the end of Li extraction.[9,10] In contrast, TEM images of cycled 1 mol% W-LNO electrodes prove that the rocksalt grains on the periphery experienced hardly any structural degradation during cycling. High-resolution TEM ([001] rocksalt zone) images in Fig. 7 showed no appreciable surface damage after cycling, and the cubic lattice was well preserved right to the outer edge. It appears that the degradation mechanism of the LNO cathodes is likely due to structural deterioration resulting from the attacks of electrolyte solution species on the active mass, which intensifies due to cracking. In addition, formation of reactive Ni^{4+} ions formed by delithiation destabilizes the crystal structure.[18] Such ions can also oxidize solvent molecules, and this possibility becomes more plausible as the particles surface area increases upon cycling due to cracking. Hence, the presence of the rocksalt phase segregated at the surface (due to doping by W) protects the cathode active mass from detrimental reactions with solution species and improves the cycling stability, possibly because the presence of Ni^{2+} ions in the rocksalt structure retards the formation of destabilizing and oxidizing Ni^{4+} ions. Overall, the electrochemical measurements, impedance spectroscopic data and post mortem analysis after cycling all demonstrate the unique stability achieved due to doping with W.

This positive effect of doping can be understood in light of structural, spectral and computational studies that suggest that such doping intensifies the presence of a rocksalt ($Fm\bar{3}m$) phase near the surface, which protects the main hexagonal $R\bar{3}m$ phase. Among all these materials, the most promising one is the W-doped LNO, which delivers the highest specific capacity and with which the stabilization effect of doping with W is the most pronounced.

4. Conclusions

The enhancement in cycling stability by W-doping appears to generally apply to all classes of Ni-rich layered cathodes and greatly alleviates the hurdles faced by the Ni-enrichment strategy, which increases the energy density of the layered cathodes but is also impaired by instability and capacity fading. Meaningful structural, spectral and computational analyses of the effect of doping by tungsten were conducted only with pure LNO cathodes (no interference by the other transition metal elements). However, rocksalt formation may be the reason for the stabilization of all types of W-doped Ni-rich layered cathode materials. Further stabilization of W-LNO cathodes beyond what was presented herein seems to be possible. Making LNO a practical cathode material with a specific capacity approaching 245 mA h g^{-1} will revolutionize the performance of Li-ion batteries in terms of energy density without affecting their safety due to the need to apply a high charging voltage. A first significant step towards this goal is demonstrated herein since the proposed W-doped Ni-rich layered cathodes clearly outperform other Ni-rich layered cathodes reported in previous publication as illustrated in Fig. S9 and Table S3 (ESI†).

Author contributions

Y.-K. Sun designed the experiments; U.-H. Kim, D.-W. Jun, and K.-J. Park synthesized and tested the cathode materials; C. M. Wang, P. Yang, and C. S. Yoon performed and analyzed the TEM imaging experiments; D. Ahn performed and analyzed the X-ray measurements; N. Leifer and G. Goobes performed the NMR; Q. Zhang, P. Kaghazchi, D. T. Major, and M. Dixit were responsible for the theoretical computations, Y.-K. Sun, C. S. Yoon, K.-H. Kim, and D. Aurbach supervised the project; Y.-K. Sun, C. S. Yoon, P. Kaghazchi, and D. Aurbach wrote the paper. All of the authors discussed the results and reviewed the manuscript.

Conflicts of interest

There are no conflicts to declare.

Acknowledgements

This work was mainly supported by the Global Frontier R&D Program (2013M3A6B1078875) on Center for Hybrid Interface Materials (HIM) funded by the Ministry of Science, the Human

Resources Development program (No. 20154010200840) of the Korea Institute of Energy Technology Evaluation and Planning (KETEP) grant funded by the Korea government Ministry of Trade. Q. Z. and P. K. gratefully acknowledge supports from the ''China Scholarship Council'' (CSC) and ''Bundesministerium füur Bildung und Forschung'' (BMBF). Q. Z and P. K. also acknowledge the North-German Supercomputing Alliance (HLRN) for providing HPC resources. High resolution X-ray diffractions experiments at PLS-II were supported by MSIP. Partial support was also obtained by the Israel Committee for High Education and the Israel Prime Minister Office in the framework of the INREP project.

Notes and references

1 D.-l. Ma, Z.-y. Cao, H.-g. Wang, X.-l. Huang, L.-m. Wang and X.-b. Zhang, *Energy Environ. Sci.*, 2012, **5**, 8538.
2 X.-l. Huang, R.-z. Wang, D. Xu, Z.-l. Wang, H.-g. Wang, J.-j. Xu, Z. Wu, Q.-c. Liu, Y. Zhang and X.-b. Zhang, *Adv. Funct. Mater.*, 2013, **23**, 4345.
3 X.-l. Huang, D. Xu, S. Yuan, D.-l. Ma, S. Wang, H.-y. Zheng and X.-b. Zhang, *Adv. Mater.*, 2014, **26**, 7264.
4 H.-G. Wang, S. Yuan, D.-L. Ma, X.-B. Zhang and J.-M. Yan, *Energy Environ. Sci.*, 2015, **8**, 1660.
5 T. Sun, Z.-j. Li, H.-g. Wang, D. Bao, F.-l. Meng and X.-b. Zhang, *Angew. Chem.*, 2016, **128**, 10820.
6 H.-J. Noh, S. Youn, C. S. Yoon and Y.-K. Sun, *J. Power Sources*, 2013, **233**, 121.
7 J. R. Dahn, U. von Sacken and C. A. Michal, *Solid State Ionics*, 1990, **44**, 87.
8 J. R. Dahn, U. von Sacken, M. W. Juzkow and H. Al-Janaby, *J. Electrochem. Soc.*, 1991, **138**, 2207.
9 T. Ohzuku, A. Ueda and M. Nagayama, *J. Electrochem. Soc.*, 1993, **140**, 1862.
10 H. Arai, S. Okada, H. Ohusuka, M. Ichimura and J. Yamaki, *Solid State Ionics*, 1995, **80**, 261.
11 M. R. Palacin, D. Larcher, A. Audemer, N. Sac-Epee, G. G. Amatucci and J.-M. Tarascon, *J. Electrochem. Soc.*, 1997, **144**, 4226.
12 W. Li, J. N. Reimers and J. R. Dahn, *Phys. Rev. B: Condens. Matter Mater. Phys.*, 1992, **46**, 3236.
13 T. Ohzuku, A. Ueda, M. Nagayama, Y. Iwakoshi and H. Komori, *Electrochim. Acta*, 1993, **38**, 1159.
14 H. Arai, S. Okada, Y. Sakurai and J.-i. Yamaki, *J. Electrochem. Soc.*, 1997, **144**, 3117.
15 L. Croguennec, E. Suard, P. Willmann and C. Delmas, *Chem. Mater.*, 2002, **14**, 2149.
16 A. Hirano, R. Kanno, Y. Kawamoto, Y. Takeda, K. Yamaura, M. Takano, K. Ohyama, M. Ohashi and Y. Yamaguchi, *Solid State Ionics*, 1995, **78**, 123.
17 A. Rougier, P. Gravereau and C. Delmas, *J. Electrochem. Soc.*, 1996, **143**, 1168.
18 D. Aurbach, K. Gamolsky, B. Markovsky, G. Salitra, Y. Gofer, U. Heider, R. Oesten and M. Schmidt, *J. Electrochem. Soc.*, 2000, **147**, 1322.
19 B.-B. Lim, S.-J. Yoon, K.-J. Park, C. S. Yoon, S.-J. Kim, J. J. Lee and Y.-K. Sun, *Adv. Funct. Mater.*, 2015, **25**, 4673.
20 J. H. Lee, C. S. Yoon, J.-Y. Hwang, S.-J. Kim., F. Maglia, P. Lamp, S.-T. Myung and Y.-K. Sun, *Energy Environ. Sci.*, 2016, **9**, 2152.
21 R. Kanno, H. Kubo, Y. Kawamoto, T. Kamiyama, F. Izumi, Y. Takeda and M. Takano, *J. Solid State Chem.*, 1994, **110**, 216.
22 B. Li, A. Michaelides and M. Scheffler, *Phys. Rev. B: Condens. Matter Mater. Phys.*, 2007, **76**, 075401.
23 R. S. Koster, C. M. Fang, M. Dijkstra, A. van Blaaderen and M. A. van Huis, *J. Phys. Chem. C*, 2015, **119**, 5648.
24 D. Kramer and G. Ceder, *Chem. Mater.*, 2009, **21**, 3799.
25 J. C. Garcia, J. Bareño, J. Yan, G. Chen, A. Hauser, J. R. Croy and H. Iddir, *J. Phys. Chem. C*, 2017, **121**, 8290.
26 S. Watanabe, M. Kinoshita, T. Hosokawa, K. Morigaki and K. Nakura, *J. Power Sources*, 2014, **258**, 210.
27 D. P. Abraham, R. D. Twesten, M. Balasubramanian, I. Petrov, J. Mcbreen and K. Amine, *Electrochem. Commun.*, 2002, **4**, 620.
28 S.-U. Woo, B.-C. Park, C. S. Yoon, S.-T. Myung, J. Prakash and Y.-K. Sun, *J. Electrochem. Soc.*, 2007, **154**, A649.